A Robust Filtered Basis Functions Approach for Feedforward Tracking Control—With Application to a Vibration-Prone 3-D Printer

Keval S. Ramani, *Member, IEEE*, Nosakhare Edoimioya, and Chinedum E. Okwudire, *Member, IEEE*

***Abstract*—The filtered basis functions (FBF) approach is gaining interest for feedforward tracking control of linear, especially, nonminimum phase systems. It expresses the control input to the plant as a linear combination of basis functions with unknown coefficients. The basis functions are forward filtered through the plant dynamics and the coefficients are selected such that the tracking error is minimized. This article proposes a robust FBF approach for tracking control of linear time invariant systems with known uncertainty. A robust filter is formulated as the inverse of an optimal controller that minimizes a frequency-domain cost function over the known uncertainty. The proposed robust FBF approach filters the basis functions using the robust filter in lieu of the nominal plant dynamics. Stability issues associated with the robust filter are discussed, as are the incorporation of dynamic uncertainty into the robust filter. Applied to a vibration-prone desktop 3-D printer with dynamic uncertainty, significant improvements in tracking accuracy are demonstrated using the robust FBF approach compared to the standard FBF approach.**

***Index Terms*—B-splines, nonminimum phase (NMP) system, optimal control, robust control, 3-D printing, vibration control.**

I. Introduction

TRACKING control is a fundamental problem encountered in a wide range of application domains, including manufacturing, robotics, and aerospace. The objective of tracking control is to force the output of the controlled system to follow a desired trajectory. Feedforward approaches are very important in tracking control applications, where they are often used to complement feedback approaches. There are also several applications where feedforward is the only or primary recourse for tracking control, e.g., due to technological, practical or economic infeasibility of sensing. A good example is desktop 3-D printers where low-cost stepper motors, which have no feedback sensors, are commonly used to generate motion. Another example is industrial wafer scanners where feedforward control accounts for over 99% of control effort [1]. This article is motivated by such applications.

In the context of feedforward control, perfect tracking control can be achieved by pole-zero cancellation [2]. However, if the plant has nonminimum phase (NMP) zeros, then the resulting control trajectory can be highly oscillatory or unbounded. NMP zeros are quite prevalent in practice, especially in systems with structural flexibilities [3]–[5]. Various strategies have been devised for feedforward tracking control of NMP systems (interested readers can see literature reviews in [6]–[8]). Of the available methods, the filtered basis functions (FBF) approach has recently been gaining interest for feedforward tracking control of linear, especially NMP, systems [9]–[12]. The FBF approach expresses the control input as a linear combination of user-defined basis functions with unknown coefficients. The basis functions are forward filtered through the plant dynamics and the coefficients are selected, using an elegant least-squares solution, such that the tracking error is minimized. The FBF approach finds its origins in iterative learning control (ILC) through the work of Frueh and Phan [13] but was not applied to feedforward tracking control of NMP systems until recently [9]–[12]. Unlike most of the methods in the literature, the FBF approach is effective for a wide range of desired trajectories and plants including nonhyperbolic systems (systems with zeros on the unit circle in the z plane) [10], [12], square and nonsquare multi-input multi-output (MIMO) systems, linear time varying systems, linear parameter varying systems [14], etc.

However, the FBF approach faces at least two practical challenges. The first is that its computational cost becomes very high as the length (number of samples) in the motion trajectory increases. To overcome this challenge, a limited preview version of FBF, viz., limited preview filtered B-splines (LPFBS), was proposed by Duan *et al.* [11]. LPFBS was shown to significantly reduce the computational cost of the FBF approach without significantly sacrificing its tracking performance, allowing it to be implemented successfully on a desktop 3-D printer [11]. A second challenge is that, being a purely feedforward technique, the tracking accuracy of the FBF approach degrades in the presence of inaccuracies in the plant model or uncertainty in the plant dynamics [11].

In the presence of uncertainty in the plant dynamics, the tracking accuracy of feedforward controllers such as FBF can be

Manuscript received September 11, 2019; revised January 15, 2020; accepted March 1, 2020. Date of publication April 1, 2020; date of current version October 14, 2020. Recommended by Technical Editor T. Singh. This work was supported by the National Science Foundation—CMMI 1825133: Boosting the Speed and Accuracy of Vibration-Prone Manufacturing Machines at Low Cost Through Software. (*Corresponding author: Chinedum E. Okwudire.*)

The authors are with the Department of Mechanical Engineering, University of Michigan, Ann Arbor, MI 48109 USA (e-mail: ksramani@umich.edu; nosed@umich.edu; okwudire@umich.edu).

Color versions of one or more of the figures in this article are available online at http://ieeexplore.ieee.org.

Digital Object Identifier 10.1109/TMECH.2020.2983680

improved by complementing them with some form of feedback control. Examples include real-time feedback [15]–[17], adaptive control [18], ILC [19]–[23], etc. However, as mentioned earlier, there are a good number of situations where feedback-based techniques do not apply due to infeasibility or inadequacy of sensing. An alternative approach, therefore, is to improve the robustness of feedforward tracking controllers without relying on feedback, using *a priori* knowledge of plant uncertainty. In this regard, Wu and Zou [24] proposed a gain modulated inversion-based controller to minimize the worst case tracking error in the presence of dynamic uncertainty, which imposes bounds on the magnitude as well as phase of the uncertainty. Lunenburg [25] presented an optimal feedforward controller that minimized (in an average sense) the tracking error in the frequency domain using a conventional multiplicative uncertainty framework that bounds only the magnitude of the uncertainty. A weakness of the robust controllers proposed in [24] and [25] is that, being direct inversion feedforward controllers [26], they cannot be applied directly to nonhyperbolic plants.

In the context of the FBF approach, which is directly applicable to nonhyperbolic plants, the authors have proposed a regularized FBF approach [27] to improve the tracking accuracy of FBF in the presence of uncertainty. However, the regularized approach, which is obtained by solving a set of nonlinear-coupled equations, is not amenable to the computationally efficient LPFBS approach. Hence, from a practical standpoint, an approach that improves the robustness of FBF and at the same time retains the elegance of the least-squares solution, which facilitates LPFBS, is needed.

Hence, this article (and its preliminary version [28]) makes the following contributions to the literature.

1) It proposes a robust FBF approach that retains the elegance of the least-squares solution of the standard FBF approach by using a robust filter instead of nominal plant dynamics to filter basis functions.
2) It proposes the inverse of an optimal feedforward controller that minimizes an error cost function for known plant uncertainty as a robust filter for use in robust FBF.
3) It demonstrates the effectiveness of the proposed robust FBF approach using simulation examples and experiments on a desktop 3-D printer with dynamic uncertainty.

The rest of this article is organized as follows. Section II presents an overview of the FBF approach. Section III introduces the proposed robust FBF approach and robust filter, as well as stability issues and incorporation of dynamic uncertainty into the robust filter. The effectiveness of the robust FBF approach is demonstrated using simulation examples and experiments on a desktop 3-D printer in Section IV. Finally, Section V concludes this article.

II. FBF Approach

Consider the discrete-time linear time invariant (LTI) single-input single-output plant $G(z)$ shown in Fig. 1, augmented with a tracking controller $C(z)$ with overall dynamics $L(z) = C(z)G(z)$ and error dynamics $E_{ff}(z) = 1 - C(z)G(z)$. The plant $G(z)$ could represent the transfer function of an open-loop or a closed-loop controlled system [29]. This section assumes that the plant model has no uncertainty. Given a desired trajectory $y_d(k)$, where $0 \leq k \leq M$, $k \in \mathbb{Z}$, and $M+1$ is the number of discrete points in the trajectory, the objective of the tracking controller $C(z)$ is to produce a signal $u(k)$, which after passing through $G(z)$ results in an output trajectory $y(k)$ that follows the desired trajectory $y_d(k)$ as closely as possible.

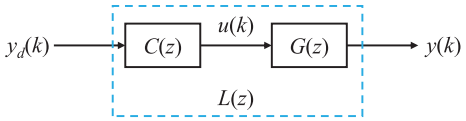

Fig. 1. Block diagram for tracking control.

The FBF approach assumes that the following conditions hold:

1) the desired trajectory $y_d(k)$ is known *a priori*, which is often the case, e.g., in manufacturing, robotics, and aeronautics applications [30];
2) the control signal $u(k)$ is expressed as a linear combination of basis functions as follows:

$$u(k) = \sum_{i=0}^{n} \gamma_i \varphi_i(k) \tag{1}$$

where $\varphi_i(k)$ and γ_i are the user-defined basis functions and their coefficients, respectively. The control input vector $\mathbf{u} = [u(0)\, u(1)\, \ldots\, u(M)]^T$ can be expressed as

$$\mathbf{u} = \mathbf{\Phi}\boldsymbol{\gamma} \tag{2}$$

where

$$\begin{aligned} \mathbf{\Phi} &= \begin{bmatrix} \boldsymbol{\varphi}_0 & \boldsymbol{\varphi}_1 & \ldots & \boldsymbol{\varphi}_n \end{bmatrix} \\ \boldsymbol{\varphi}_i &= \begin{bmatrix} \varphi_i(0) & \varphi_i(1) & \ldots & \varphi_i(M) \end{bmatrix}^T \\ \boldsymbol{\gamma} &= \begin{bmatrix} \gamma_0 & \gamma_1 & \ldots & \gamma_n \end{bmatrix}^T. \end{aligned} \tag{3}$$

The resulting output trajectory $\mathbf{y} = [y(0)\, y(1)\, \ldots\, y(M)]^T$ can be expressed as a linear combination of FBF

$$\mathbf{y} = \tilde{\mathbf{\Phi}}\boldsymbol{\gamma} \tag{4}$$

where $\tilde{\mathbf{\Phi}}$ is an $(M+1) \times (n+1)$ matrix whose columns $\tilde{\boldsymbol{\varphi}}_i$ are obtained by filtering $\boldsymbol{\varphi}_i$ using a nominal model G_{nom} of the plant G, as shown in Fig. 2. The implication is that the tracking error vector $\mathbf{e}$ can be expressed as

$$\mathbf{e} = \mathbf{y}_d - \tilde{\mathbf{\Phi}}\boldsymbol{\gamma} \tag{5}$$

where $\mathbf{y}_d = [y_d(0)\, y_d(1)\, \ldots\, y_d(M)]^T$. The coefficients $\boldsymbol{\gamma}$ are selected such that an objective function J, representing the 2-norm of the tracking error, is minimized, i.e.

$$\min_{\boldsymbol{\gamma}} \left[J = \|\mathbf{e}\|_2 = \left\| \tilde{\mathbf{\Phi}}\boldsymbol{\gamma} - \mathbf{y}_d \right\|_2 \right] \tag{6}$$

the result is an optimal coefficient vector $\boldsymbol{\gamma}$ given by

$$\boldsymbol{\gamma} = \left(\tilde{\mathbf{\Phi}}^T \tilde{\mathbf{\Phi}} \right)^{-1} \tilde{\mathbf{\Phi}}^T \mathbf{y}_d. \tag{7}$$

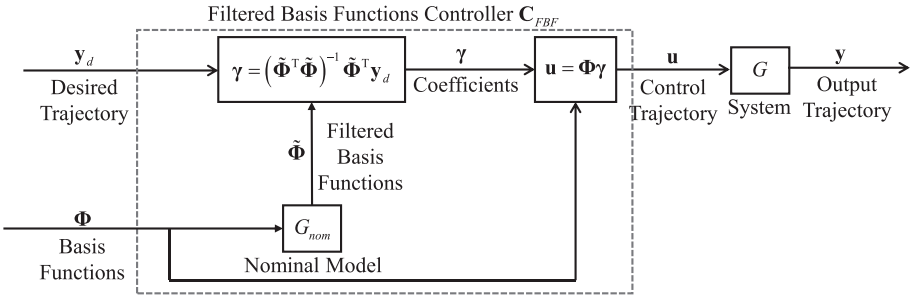

Fig. 2. Flowchart for the standard FBF approach.

Accordingly, the FBF controller $\mathbf{C}_{\mathrm{FBF}}$ and overall dynamics $\mathbf{L}_{\mathrm{FBF}}$ can be expressed as

$$\mathbf{C}_{\mathrm{FBF}} = \boldsymbol{\Phi}\left(\tilde{\boldsymbol{\Phi}}^T\tilde{\boldsymbol{\Phi}}\right)^{-1}\tilde{\boldsymbol{\Phi}}^T; \quad \mathbf{L}_{\mathrm{FBF}} = \tilde{\boldsymbol{\Phi}}\left(\tilde{\boldsymbol{\Phi}}^T\tilde{\boldsymbol{\Phi}}\right)^{-1}\tilde{\boldsymbol{\Phi}}^T. \quad (8)$$

Remark 1: It can be shown (see [10]) that $\mathbf{C}_{\mathrm{FBF}}$ is an approximation of G_{nom}^{-1}, where $\mathbf{G}_{\mathrm{nom}}$ is the lifted system representation (LSR) of G_{nom}. As $n \to M$, $\mathbf{C}_{\mathrm{FBF}} \to \mathbf{G}_{\mathrm{nom}}^{-1}$. However, $n = M$ leads to unstable G_{nom}^{-1} in the presence of NMP zeros in G_{nom}. Hence, $n < M$ is typically used to bound the control effort produced by $\mathbf{C}_{\mathrm{FBF}}$.

III. Robust FBF Approach

A. Definition of Robust Filter

The standard FBF controller discussed in the previous section assumes that the nominal model, G_{nom}, is a perfect representation of the actual plant, G. However, in practice, $G \neq G_{\mathrm{nom}}$, due to uncertainty. In this section, we propose a robust FBF approach that replaces G_{nom} in the standard FBF approach with a robust filter, G_r, which considers the uncertainty in G.

In the presence of uncertainty in G, the optimal tracking controller has been proposed in the literature [25] as the controller that minimizes the following cost function (at each frequency, ω) over the uncertainty:

$$J_r = \int_{\Delta} f(\Delta)\,|E_{ff}|^2 d\Delta; \quad E_{ff} = 1 - CG \quad (9)$$

where $f(\Delta)$ is the distribution of the actual plant G w.r.t. the uncertainty Δ. Note that for simplicity of notation, the dependence of $f(\Delta)$ and E_{ff} on ω is not explicitly shown in (9) and in the following equations. The optimal controller can be obtained by differentiating J_r w.r.t. C^* and equating the result to zero, where the superscript $*$ denotes the complex conjugate. The optimal controller is given by

$$C_{opt} = \frac{\int_{\Delta} f(\Delta)\,G^* d\Delta}{\int_{\Delta} f(\Delta)\,GG^* d\Delta}. \quad (10)$$

The goal of robust FBF is for $\mathbf{C}_{\mathrm{FBF}}$ defined in (8) to emulate $\mathbf{C}_{\mathrm{opt}}$ (the LSR of C_{opt}). To do this, we note from Remark 1 that $\mathbf{C}_{\mathrm{FBF}}$ approximates the inverse of the dynamics used to filter the basis functions Φ. In the case of the standard FBF, it approximates $\mathbf{G}_{\mathrm{nom}}^{-1}$, because G_{nom} is used to filter Φ. Therefore, to make $\mathbf{C}_{\mathrm{FBF}}$ to approximate $\mathbf{C}_{\mathrm{opt}}$, we propose a robust filter G_r as

$$G_r \triangleq C_{\mathrm{opt}}^{-1} = \frac{\int_{\Delta} f(\Delta)\,GG^* d\Delta}{\int_{\Delta} f(\Delta)\,G^* d\Delta}. \quad (11)$$

By filtering Φ using G_r instead of G_{nom}, $\mathbf{C}_{\mathrm{FBF}} \to \mathbf{C}_{\mathrm{opt}}$ as $n \to M$. Accordingly, referring to Fig. 2, the robust FBF approach simply replaces G_{nom} in the standard FBF by G_r. Hence, the proposed robust FBF approach retains the elegance of the least-squares solution of the standard FBF approach, which facilitates LPFBS.

B. Implications of NMP Behavior of Robust Filter

One may wonder why one should emulate or approximate C_{opt} using robust FBF instead of simply employing C_{opt} as a standalone controller. A major reason is that C_{opt} could be unstable, even if G is stable [25]. In such a case, the unstable poles in C_{opt} become NMP zeros in G_r, which are handled effectively by the FBF approach, regardless of their location in the complex plane (including zeros on the unit circle [10], [11], [31].

However, C_{opt} could also have NMP zeros, even if G is minimum phase (MP). The implication is that G_r would have unstable poles, yielding unstable FBF that are detrimental to the robust FBF approach. This section demonstrates this challenge using a simple first-order plant with parametric uncertainty and proposes an approach to tackle it.

Consider the first-order plant [32] in the following, consisting a real stable pole p, whose location in the z plane is known precisely, and a real zero a, whose location in the z plane is not known accurately but belongs to a set as follows:

$$G(z) = \frac{z-a}{z-p}; \quad a \in [a_l, a_h] \quad (12)$$

where a_l and a_h are lower and upper limits on zero location, respectively. Substituting (12) in (11) (assuming uniform distribution of uncertainty, $f(\Delta) = f(a) = 1$) gives

$$G_r(z) = \frac{z^2 - \left(a_{\mathrm{nom}} + \frac{1}{a_{\mathrm{nom}}} + \frac{a_d^2}{3a_{\mathrm{nom}}}\right)z + 1}{(z-p)\left(z - \frac{1}{a_{\mathrm{nom}}}\right)} \quad a_{\mathrm{nom}} \neq 0$$

$$a_{\mathrm{nom}} \triangleq \frac{a_h + a_l}{2}; \quad a_d \triangleq \frac{a_h - a_l}{2}. \quad (13)$$

Proposition 1: For $a_d > 0$, the robust filter given by (13) has two distinct real zeros, one of which lies inside the unit circle and the other outside the unit circle in the z plane.

Proof:

Since

$$\min\left(\left|a_{\text{nom}} + \frac{1}{a_{\text{nom}}}\right|\right) = 2 \tag{14}$$

and $a_d^2/3a_{\text{nom}}$ has same sign as $a_{\text{nom}} + 1/a_{\text{nom}}$, one can conclude that

$$\left|a_{\text{nom}} + \frac{1}{a_{\text{nom}}} + \frac{a_d^2}{3a_{\text{nom}}}\right| > 2$$

$$\Rightarrow \left(a_{\text{nom}} + \frac{1}{a_{\text{nom}}} + \frac{a_d^2}{3a_{\text{nom}}}\right)^2 > 4. \tag{15}$$

The implication of (15) is that the discriminant corresponding to the zeros of G_r is greater than zero and hence, G_r has two distinct real zeros.

Since the product of the roots of a quadratic equation is equal to the constant term divided by the leading coefficient, one can conclude that the product of the two zeros is one. Therefore, one zero lies outside the unit circle, whereas, the other lies inside the unit circle in the z plane. ■

The robust filter G_r can be expressed as

$$G_r(z) = \underbrace{\frac{z - a_{\text{nom}}}{z - p}}_{G_{\text{nom}}(z)} \underbrace{\frac{z^2 - \left(a_{\text{nom}} + \frac{1}{a_{\text{nom}}} + \frac{a_d^2}{3a_{\text{nom}}}\right) z + 1}{(z - a_{\text{nom}})\left(z - \frac{1}{a_{\text{nom}}}\right)}}_{\alpha(z)} \tag{16}$$

which implies that it is obtained by gain modulation of the nominal plant model. Note that $\alpha(z) = 1$ and $G_r(z) = G_{\text{nom}}(z)$ for $a_d = 0$. The implication is that in the absence of uncertainty, the robust filter is the nominal model. Notice that the robust filter G_r has an NMP zero irrespective of whether the nominal plant is NMP or MP. Also, the robust filter has two poles—one of which is stable, whereas the stability of the other depends on whether the nominal plant is NMP or MP. The robust filter is stable if the nominal plant is NMP and unstable if the nominal plant is MP. The unstable pole is a challenge for using G_r in robust FBF.

Remark 2: The optimal controller C_{opt} [inverse of the robust filter G_r given by (16)] is obtained by gain modulating the inverse of the nominal model. To ensure gain modulation, the poles and zeros should mirror each other in the z plane w.r.t. the unit circle. Mirroring results in an NMP controller if the nominal plant is MP and an MP controller if the nominal plant is NMP. Similar behavior has also been observed in the literature, for example, the popular zero phase error tracking controller [2] has NMP zero(s) if the plant is MP and MP zero(s) if the plant is NMP.

To address the instability of G_r, we propose filtering the basis functions with G_r using a strategy similar to the stable inversion approach [25], [26]. The filter G_r is decomposed into stable and unstable dynamics. The basis functions are filtered through the stable dynamics using past information (forward in time domain), and filtered through unstable dynamics using preview (backward in time). Once the basis functions are filtered, the remaining process to obtain the coefficients and the control input is identical to the one described in Section II. However, the above-described filtering approach cannot handle poles on the unit circle. One possible solution for poles on the unit circle is to replace them with slightly perturbed poles that are close to but not on the unit circle [33].

C. Consideration of Dynamic Uncertainty and Uncertainty Distribution

The first-order example in the previous section considered parametric uncertainty with uniform distribution. However, in practice, uncertainty is typically dynamic in nature and its distribution is not uniform [11], [24], [25]. Hence, this section presents an approach to incorporate dynamic uncertainty and a versatile kernel distribution into the formulation of the robust filter.

In the presence of dynamic uncertainty, the actual plant can be expressed as

$$G(\omega) = r(\omega)\, e^{j\theta(\omega)}$$
$$r(\omega) \in [r_{\min}(\omega),\ \ r_{\max}(\omega)]\,;\ \ \theta(\omega) \in [\theta_{\min}(\omega),\ \ \theta_{\max}(\omega)] \tag{17}$$

where j is the unit imaginary number, r is the magnitude of the actual plant, θ is the phase of the actual plant, ω is the frequency in rad/s, and the subscripts "max" and "min" denote upper and lower bounds. Fig. 3(a) and (b) illustrates G using the Bode plot and the complex plane.

The distribution of uncertainty $f(\Delta) = f(r,\theta)$ can take different forms, and can be described using various types of uncertainty distribution models, e.g., normal, uniform, Rayleigh, etc. Here, without loss of generality, we propose a kernel distribution (with normal kernels) because of its versatility in describing various types of uncertainty distributions [34]. The kernel distribution is defined as follows (for frequency ω):

$$f(r,\theta) = f_1(r)\, f_2(\theta)$$
$$f_1(r) = \frac{1}{l\sigma_r}\sum_{i=1}^{l} K\left(\frac{r - r_i}{\sigma_r}\right) = \frac{1}{\sqrt{2\pi} l\sigma_r^2}\sum_{i=1}^{l} e^{-\frac{(r-r_i)^2}{2\sigma_r^2}}$$
$$f_2(\theta) = \frac{1}{l\sigma_\theta}\sum_{i=1}^{l} K\left(\frac{\theta - \theta_i}{\sigma_\theta}\right) = \frac{1}{\sqrt{2\pi} l\sigma_\theta^2}\sum_{i=1}^{l} e^{-\frac{(\theta-\theta_i)^2}{2\sigma_\theta^2}} \tag{18}$$

where indices $i = 1, 2, \ldots, l$ denote frequency response functions (FRFs) sampled from G, corresponding to the different operating conditions; l is the total number of FRF samples; K is the normal kernel with mean values $(r_i,\ \theta_i)$ and standard deviations $(\sigma_r,\ \sigma_\theta)$. The mean values r_i and θ_i are the magnitude and phase of the ith FRF at frequency ω, respectively. For a given frequency ω, the standard deviations σ_r and σ_θ are identical for all l kernels. Fig. 3(c) depicts an example of individual normal kernels and their summation. Substituting function $f(r,\theta)$ defined by (18) and uncertainty given by (17) into (11), the robust filter can be

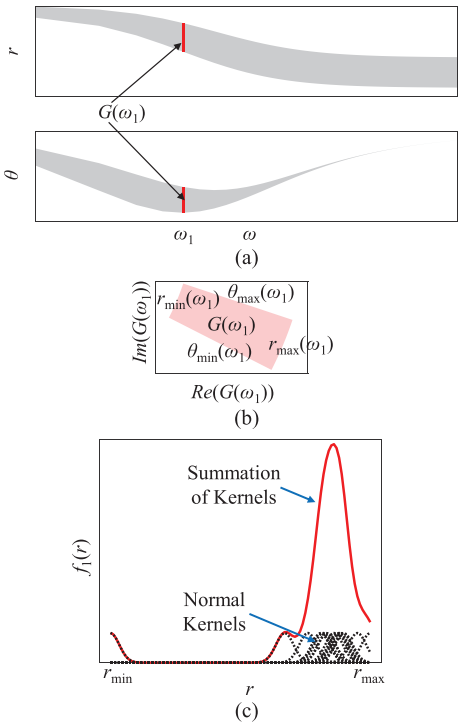

Fig. 3. Illustration of dynamic uncertainty using (a) Bode plot, (b) complex plane, and (c) kernel distribution.

expressed as

$$G_r = \frac{\left\{\sum_{i=1}^{l} \alpha_{ri}\right\}\left\{\sum_{i=1}^{l} \alpha_{\theta i}\right\}}{\left\{\sum_{i=1}^{l} \beta_{ri}\right\}\left\{\sum_{i=1}^{l} \beta_{\theta i}\right\}}$$

$$\alpha_{ri} \triangleq \int_{r_{\min}}^{r_{\max}} K\left(\frac{r-r_i}{\sigma_r}\right) r^3 dr,\ \alpha_{\theta i} \triangleq \int_{\theta_{\min}}^{\theta_{\max}} K\left(\frac{\theta-\theta_i}{\sigma_\theta}\right) d\theta$$

$$\beta_{ri} \triangleq \int_{r_{\min}}^{r_{\max}} K\left(\frac{r-r_i}{\sigma_r}\right) r^2 dr,\ \beta_{\theta i} \triangleq \int_{\theta_{\min}}^{\theta_{\max}} K\left(\frac{\theta-\theta_i}{\sigma_\theta}\right) e^{-j\theta} d\theta. \tag{19}$$

Remark 3: Wu and Zou [24] designed an optimal controller in the presence of dynamic uncertainty [given by (17)] using worst case optimization, but assumed a gain modulated inversion structure for their optimal controller. To improve the worst case tracking error using FBF, the inverse of the optimal controller proposed by Wu and Zou [24] can be used as the filter G_r, similar to (11).

IV. Application to a Desktop 3-D Printer

A. Setup for Simulations and Experiments

To keep their weight and costs low, commercial desktop 3-D printers incorporate timing belts and lightweight components, which introduce structural flexibilities into their dynamics. Hence, manufactured parts suffer from surface waviness and registration errors caused by excess vibration, especially when high-acceleration motions are commanded [11]. Moreover, they are driven in an open loop by stepper motors. Hence, they cannot sense and counteract the motion-induced vibration via feedback control. Feedforward methods like the FBF approach can mitigate these vibrations by modifying the motion commands sent to the 3-D printer and improving the accuracy of the parts, without incurring any additional costs from feedback sensors. Up to 54% reduction in printing time, without sacrificing accuracy, has been demonstrated using the FBF method to compensate desktop 3-D printer vibration in feedforward [35]. However, significant uncertainty in system dynamics and its adverse effects on printing accuracy has also been observed [11].

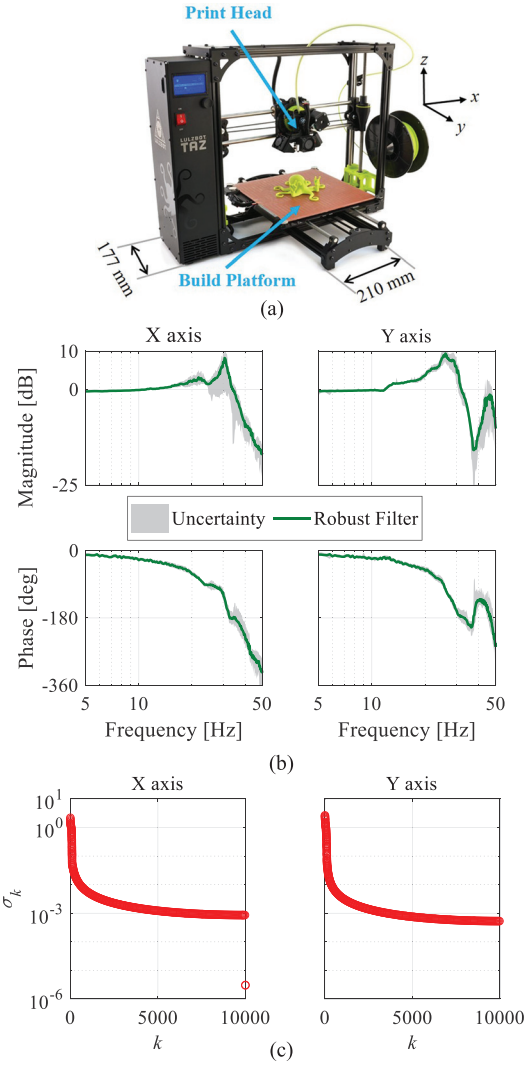

Fig. 4. (a) Lulzbot Taz 6 desktop 3-D printer. (b) FRFs corresponding to dynamic uncertainty and robust filter. (c) Singular values of LSR of *x*- and *y*-axes robust filters showing NMP behavior in *x*-axis.

This section validates the robust FBF approach using simulations and experiments on a Lulzbot Taz 6 desktop 3-D printer, as shown in Fig. 4(a). For system identification and control, motion commands are sent to the printer's stepper motors at 1-kHz sampling rate using a real-time controller (dSPACE 1202) via stepper motor drivers (Pololu DRV8825).

The FRFs of the 3-D printer are obtained by applying swept sine acceleration signals (with amplitudes ranging from 2 to

5 m/s^2 in increments of 0.2 m/s^2) to the printer's stepper motors (each having 10-μm stepping resolution) and measuring the relative acceleration of the build platform and print head using accelerometers (SparkFun ADXL335 triple-axis). The uncertainty region shown in Fig. 4(b) represents the variations in magnitude and phase of the measured FRFs as functions of input acceleration amplitude.

The standard deviations σ_r and σ_θ for the normal kernels are estimated optimally from FRF data using the *fitdist* function in MATLAB. Using (19), the robust filters for the x- and y-axes are obtained and their FRFs are shown in Fig. 4(b). Fig. 4(c) shows the singular values of the LSRs of the robust filters. Singular values of the LSR provide information about stability and NMP behavior of the corresponding dynamics. Very high and small values of the singular values, which deviate from the cluster, denote the presence of unstable pole(s) and NMP zeros(s), respectively (for details about LSR and its singular values see [31], [36]). In Fig. 4(c), since the highest singular values do not deviate from the cluster of singular values, the robust filters are stable. However, the two smallest singular values for the x-axis deviate from the cluster, which implies that the robust filter for the x-axis has a pair of complex NMP zeros.

B. Simulations

As discussed in Sections II and III, the basis functions are user-defined and there is a wide range of basis functions available for use with the standard FBF and robust FBF methods, e.g., Laguerre functions [37], wavelets [38], etc. This section uses the B-splines [9] because they are commonly used to parameterize commands sent to manufacturing machines and robots [30]. For a B-spline of degree m, having $n+1 \leq M+1$ control points (same as coefficients of basis functions), $\gamma_0, \gamma_1, \ldots, \gamma_n$, and knot vector $[\eta_0\, \eta_1\, \ldots\, \eta_{m+n+1}]^T$, its real-valued basis functions, $\varphi_{i,m}$, are given by [39]

$$\begin{aligned}\varphi_i(k) &:= \varphi_{i,m}(\xi_k) \\ &= \frac{\xi_k - \eta_i}{\eta_{i+m} - \eta_i}\varphi_{i,m-1}(\xi) + \frac{\eta_{i+m+1} - \xi_k}{\eta_{i+m+1} - \eta_{i+1}}\varphi_{i+1,m-1}(\xi) \\ \varphi_{i,0}(\xi_k) &= \begin{cases} 1 & \eta_i \leq \xi_k \leq \eta_{i+1} \\ 0 & \text{otherwise} \end{cases} \end{aligned} \tag{20}$$

where $i = 0, 1, \ldots, n$ with $\xi_k \in [0, 1]$, representing normalized time, discretized into $M+1$ points, $\xi_0, \xi_1 \ldots \xi_M$, and η_j is a uniform knot vector, selected such that

$$\eta_j = \begin{cases} 0 & 0 \leq j \leq m \\ \frac{j-m}{n-m+1} & m+1 \leq j \leq n \\ 1 & n+1 \leq j \leq m+n+1. \end{cases} \tag{21}$$

For comparison of robust FBF with standard FBF, a signal with frequency content uniformly distributed between 5 and 50 Hz, along the x-axis, is used as the desired trajectory. The length of the desired trajectory is 1 s, resulting in 1001 discrete points (i.e., $M = 1000$) based on sampling time $T_s = 1$ ms. For each acceleration magnitude shown in Fig. 5, the basis functions are filtered with the corresponding FRF to generate a standard FBF controller for that particular FRF. The robust FBF and each case of the standard FBF approach is simulated for 10 000 realizations of G (generated using the kernel distribution specified by function $f(r, \theta)$), along the x-axis. B-splines with parameters $m = 5$ and $n = 200$ are used as basis functions. The performance of the robust FBF relative to standard FBF approach is quantified by the following metric q:

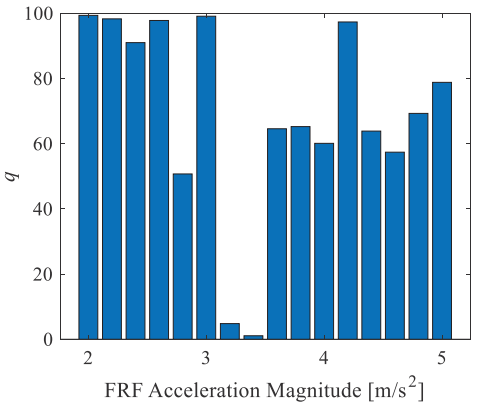

Fig. 5. Bar graph showing metric defined in (22) for different FRFs based on simulations of 10 000 realizations of the actual plant dynamics of the x-axis using B-splines basis functions ($n = 200$, $M = 1000$).

$$q = \frac{\text{mean}(e_{\text{RMS},S}) - \text{mean}(e_{\text{RMS},R})}{\text{mean}(e_{\text{RMS},S})} \times 100 \tag{22}$$

where $e_{\text{RMS},S}$ and $e_{\text{RMS},R}$ denote the root mean square (RMS) errors corresponding to standard and robust FBF, respectively, for the 10 000 realizations of G. Fig. 5 plots q for each FRF acceleration magnitude. It is seen that robust FBF outperforms the standard FBF approach by factors ranging from 1% to 99%, depending on the FRF acceleration magnitude.

Remark 4: It has been shown in Section IV-A that the robust filters for the 3-D printer are stable. To demonstrate the effectiveness of the proposed approach for unstable robust filters and to validate the discussion in Section III-B, simulation examples are presented in Appendix A.

C. Experiments

The model shown in Fig. 6 is printed using the 3-D printer, shown in Fig. 4(a), with a maximum speed of 130 mm/s and acceleration limits of 3 m/s^2, 4 m/s^2 and 5 m/s^2 imposed separately on the desired trajectory. To generate the axis-level commands, the controller reads a G-code file (generated using Cura software package) and parses the G-code information into axis-level commands. The model is printed using robust FBF as well as standard FBFs (using FRFs corresponding to 3 m/s^2, 4 m/s^2 and 5 m/s^2). Since the length of the desired trajectory is large, the parts are printed using the limited preview version of FBF using B-splines, i.e., LPFBS. The LPFBS parameters are $n_{\text{up}} = 28$, $n_C = 56$, $L_C = 952$, $m = 5$, $L = 17$ (for more details about the LPFBS approach and the parameter definitions, see Appendix B). For each printed model, the thickness x of each of the 24 triangles is measured using Husky digital calipers (model#

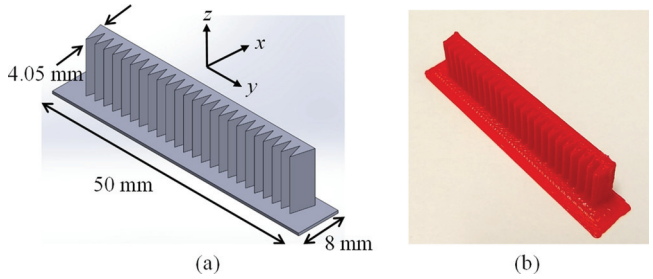

Fig. 6. (a) CAD model of the part. (b) Sample of a printed part.

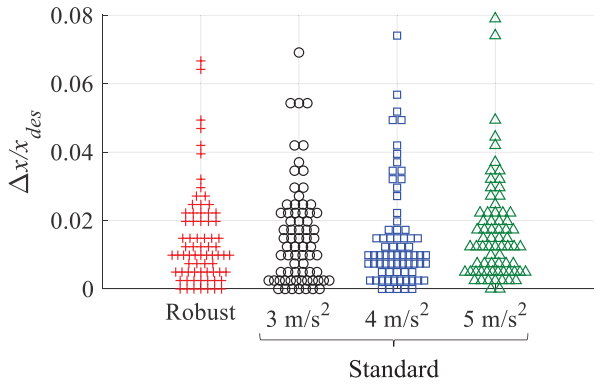

Fig. 7. Bee-swarm plot comparing the relative error in thickness of the total 72 triangles of three printed parts using robust FBF and three cases of standard FBF generated using the FRFs corresponding to the acceleration magnitudes shown in the figure.

1467H, 10-μm resolution) and compared to the desired thickness of the triangles $x_{\text{des}} = 4.05$ mm.

Fig. 7 shows a bee-swarm plot comparing the relative error ($\Delta x/x_{\text{des}}$, $\Delta x = |x_{\text{des}} - x|$) in the triangles for the robust and standard FBF (using FRFs 3 m/s^2, 4 m/s^2 and 5 m/s^2) cases. In an average sense, the robust FBF approach improves $\Delta x/x_{\text{des}}$ w.r.t. 3 m/s^2, 4 m/s^2 and 5 m/s^2 standard FBFs by 7%, 2%, and 12%, respectively. Using the worst case scenario as a metric, the robust FBF approach improves $\Delta x/x_{\text{des}}$ by 4%, 10%, and 16%, respectively, as compared to 3 m/s^2, 4 m/s^2 and 5 m/s^2 standard FBFs.

V. Conclusion

This article has proposed a robust FBF approach for feedforward tracking control of LTI systems with known uncertainty. The standard FBF approach uses a nominal model of the plant for filtering basis functions, so that the FBF controller approximates the inverse of the nominal model—the optimal controller in the absence of uncertainty. Conversely, the proposed robust FBF approach substitutes a robust filter in place of a nominal plant model. As a robust filter, this article proposes the inverse of an optimal controller obtained by minimizing a cost function over the range of known plant uncertainty. The substitution of the nominal model with the robust filter ensures that the FBF controller approximates the optimal controller in the presence of uncertainties.

Stability issues associated with the robust filter are discussed in the context of a first-order system with parametric uncertainty, and an approach for resolving them is presented. The robust and standard FBF approaches are compared in simulations and experiments using a vibration-prone desktop 3-D printer as an example. Dynamic uncertainty with a kernel distribution is used to model the uncertain 3-D printer.

The approach devised in this article for achieving robust FBF has broader implications, i.e., the FBF controller can be made to emulate any linear controller simply by filtering the basis functions with the inverse of the desired controller. This further enhances the versatility and practicality of the FBF controller. Future work will seek to extend the proposed robust filter design approach to other types of linear systems, such as linear time varying, linear parameter varying and MIMO systems, and basis function selection for robust control.

Appendix A
Simulation Results for the First-Order System

To validate the approach mentioned in Section III-B, simulations are carried out using the first-order plant with a fixed pole at $p = 0.5$ and nominal real zero locations $|a_{\text{nom}}| \in \{0.99, 1, 1.01\}$. Nominal zero locations $|a_{\text{nom}}| = 0.99$ and 1.01 yield G_r with unstable and stable poles close to the unit circle, respectively. The uncertainty parameter $a_d = 0.1$ and the desired trajectory y_d is a zero-mean white noise signal with variance equal to 1, $M = 1000$ and sampling frequency 10 kHz. B-spline basis functions with $n = 990$ are used in this example. For $|a_{\text{nom}}| > 1$, G_r is stable and the basis functions are filtered forward in time. Conversely, for $|a_{\text{nom}}| < 1$, G_r is unstable and the basis functions are filtered forward and backward in time, as described in Section III-B. When $|a_{\text{nom}}| = 1$, G_r has a marginally stable pole, which cannot

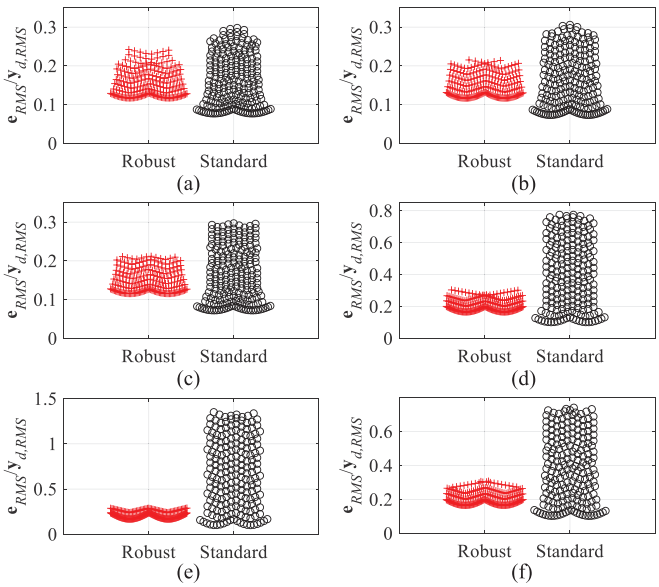

Fig. 8. Bee-swarm plots comparing normalized RMS error of standard and robust FBF approaches for simple first-order plant with parametric uncertainty (a_{nom} = (a) –1.01, (b) –1, (c) –0.99, (d) 0.99, (e) 1, and (f) 1.01, $a_d = 0.1$) for 201 realizations of the plant.

be dealt with by forward or reverse filtering in time. It is dealt with by using a slightly perturbed value of $|a_{\text{nom}}| = 0.999$, for filtering. Fig. 8 shows the normalized RMS error $\mathbf{e}_{\text{RMS}}/\mathbf{y}_{d,\text{RMS}}$ for 201 realizations of the plants, using bee-swarm plots. It is observed that robust FBF has a much lower standard deviation as compared to standard FBF. In terms of mean$(\mathbf{e}_{\text{RMS}}/\mathbf{y}_{d,\text{RMS}})$, robust FBF outperforms standard FBF by 3%, 9%, 10%, 48%, 69%, and 46% for $a_{\text{nom}} = -1.01, -1, -0.99, 0.99, 1$, and 1.01, respectively.

Appendix B
Limited Preview Filtered B-Splines

This appendix presents a brief discussion on the LPFBS approach. For more details, interested readers can refer to [11]. In contrast to the full preview version of the FBF approach, the LPFBS approach generates the control input $u(k)$ using sequential batches (windows) of the desired trajectory $y_d(k)$ (see Fig. 9). Hence, the tracking problem is solved in small batches

$$\bar{\mathbf{e}} = \mathbf{y}_d - \bar{\mathbf{\Phi}}\bar{\gamma} \Leftrightarrow \begin{bmatrix} \bar{\mathbf{e}}_P \\ \bar{\mathbf{e}}_C \\ \bar{\mathbf{e}}_F \end{bmatrix} = \begin{bmatrix} \mathbf{y}_{d,P} \\ \mathbf{y}_{d,C} \\ \mathbf{y}_{d,F} \end{bmatrix} - \begin{bmatrix} \bar{\mathbf{\Phi}}_P & \mathbf{0} & \mathbf{0} \\ \bar{\mathbf{\Phi}}_{PC} & \bar{\mathbf{\Phi}}_C & \mathbf{0} \\ \mathbf{0} & \bar{\mathbf{\Phi}}_{CF} & \bar{\mathbf{\Phi}}_F \end{bmatrix} \begin{bmatrix} \bar{\gamma}_P \\ \bar{\gamma}_C \\ \bar{\gamma}_F \end{bmatrix} \tag{23}$$

where subscripts "*P*," "*C*," and "*F*" denote the past, current, and future batches, respectively, and the bar on the matrices and vectors indicates that the impulse response of the FRF used for filtering the B-splines is truncated. Using local least squares, the coefficients of the current batch can be approximated as

$$\bar{\gamma}_C \cong \left(\bar{\mathbf{\Phi}}_C^T \bar{\mathbf{\Phi}}_C\right)^{-1} \bar{\mathbf{\Phi}}_C^T \left(\mathbf{y}_{d,C} - \bar{\mathbf{\Phi}}_{PC}\bar{\gamma}_P\right) \tag{24}$$

where $\overline{\gamma_P}$ denote coefficients calculated in the past batch. Note that information from the future batch is not considered while calculating coefficients for the current batch. In this manner, using (24) coefficients are computed for the moving window. The dimensions of the current window are defined by L_C and n_C, where L_C is the number of trajectory points considered in the current batch and n_C is the number of coefficients. Note that although n_C coefficients are computed, only n_{up} are updated in each window. The parameter L denotes the knot vector spacing.

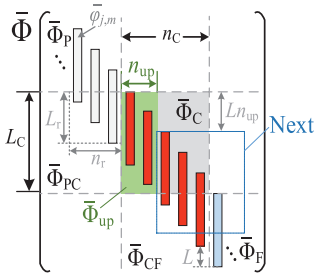

Fig. 9. Illustration for LPFBS.

References

[1] D. Bruijnen and N. van Dijk, "Combined input shaping and feedforward control for flexible motion systems," in *Proc. Amer. Control Conf.*, 2012, pp. 2473–2478.

[2] M. Tomizuka, "Zero phase error tracking algorithm for digital control," *J. Dyn. Syst. Meas. Control*, vol. 109, no. 1, pp. 65–68, 1987.

[3] K. Astrom and B. Wittenmark, *Computer Controlled Systems: Theory and Design*. Englewood Cliffs, NJ, USA: Prentice-Hall, 1984.

[4] D. K. Miu, *Mechatronics: Electromechanics and Contromechanics*. New York, NY, USA: Springer, 2012.

[5] H. M. Van Brussel, "Mechatronics—A powerful concurrent engineering framework," *IEEE/ASME Trans. Mechatronics*, vol. 1, no. 2, pp. 127–136, Jun. 1996.

[6] G. M. Clayton, S. Tien, K. K. Leang, Q. Zou, and S. Devasia, "A review of feedforward control approaches in nanopositioning for high-speed SPM," *J. Dyn. Syst. Meas. Control*, vol. 131, no. 6, 2009, Art. no. 061101.

[7] B. P. Rigney, L. Y. Pao, and D. A. Lawrence, "Nonminimum phase dynamic inversion for settle time applications," *IEEE Trans. Control Syst. Technol.*, vol. 17, no. 5, pp. 989–1005, Sep. 2009.

[8] J. van Zundert and T. Oomen, "On inversion-based approaches for feedforward and ILC," *Mechatronics*, vol. 50, pp. 282–291, 2018.

[9] M. Duan, K. S. Ramani, and C. E. Okwudire, "Tracking control of non-minimum phase systems using filtered basis functions: A NURBS-based approach," in *Proc. ASME Dyn. Syst. Control Conf.*, 2015, Paper V001T03A006.

[10] K. S. Ramani, M. Duan, C. E. Okwudire, and A. G. Ulsoy, "Tracking control of linear time-invariant nonminimum phase systems using filtered basis functions," *J. Dyn. Syst. Meas. Control*, vol. 139, no. 1, 2017, Art. no. 011001.

[11] M. Duan, D. Yoon, and C. E. Okwudire, "A limited-preview filtered B-spline approach to tracking control—With application to vibration-induced error compensation of a commercial 3D printer," *Mechatronics*, vol. 56, pp. 287–296, 2018.

[12] R. Romagnoli and E. Garone, "A general framework for approximated model stable inversion," *Automatica*, vol. 101, pp. 182–189, 2019.

[13] J. A. Frueh and M. Q. Phan, "Linear quadratic optimal learning control (LQL)," *Int. J. Control*, vol. 73, no. 10, pp. 832–839, 2000.

[14] Y. Kasemsinsup, R. Romagnoli, M. Heertjes, S. Weiland, and H. Butler, "Reference-tracking feedforward control design for linear dynamical systems through signal decomposition," in *Proc. Amer. Control Conf.*, 2017, pp. 2387–2392.

[15] Y. Zhao and S. Jayasuriya, "Feedforward controllers and tracking accuracy in the presence of plant uncertainties," *J. Dyn. Syst. Meas. Control*, vol. 117, no. 4, pp. 490–495, 1995.

[16] L. Y. Pao, J. A. Butterworth, and D. Y. Abramovitch, "Combined feedforward/feedback control of atomic force microscopes," in *Proc. Amer. Control Conf.*, 2007, pp. 3509–3515.

[17] S. S. Aphale, S. Devasia, and S. R. Moheimani, "High-bandwidth control of a piezoelectric nanopositioning stage in the presence of plant uncertainties," *Nanotechnology*, vol. 19, no. 12, 2008, Art. no. 125503.

[18] T.-C. Tsao and M. Tomizuka, "Adaptive zero phase error tracking algorithm for digital control," *J. Dyn. Syst. Meas. Control*, vol. 109, no. 4, pp. 349–354, 1987.

[19] Y. Wu and Q. Zou, "An iterative-based feedforward-feedback control approach to high-speed atomic force microscope imaging," *J. Dyn. Syst. Meas. Control*, vol. 131, no. 6, 2009, Art. no. 061105.

[20] H. Wang, K. Kim, and Q. Zou, "B-spline-decomposition-based output tracking with preview for nonminimum-phase linear systems," *Automatica*, vol. 49, no. 5, pp. 1295–1303, 2013.

[21] R. de Rozario, A. J. Fleming, and T. Oomen, "Iterative control for periodic tasks with robustness considerations, applied to a nanopositioning stage," *IFAC-PapersOnLine*, vol. 49, no. 21, pp. 623–628, 2016.

[22] A. Tayebi, S. Abdul, M. B. Zaremba, and Y. Ye, "Robust iterative learning control design: Application to a robot manipulator," *IEEE/ASME Trans. Mechatronics*, vol. 13, no. 5, pp. 608–613, Oct. 2008.

[23] Y. Ye and D. Wang, "DCT basis function learning control," *IEEE/ASME Trans. Mechatronics*, vol. 10, no. 4, pp. 449–454, Aug. 2005.

[24] Y. Wu and Q. Zou, "Robust inversion-based 2-DOF control design for output tracking: Piezoelectric-actuator example," *IEEE Trans. Control Syst. Technol.*, vol. 17, no. 5, pp. 1069–1082, Sep. 2009.

[25] J. J. M. Lunenburg, "Inversion-based MIMO feedforward design beyond rigid body systems," Eindhoven Univ. Technol., Eindhoven, The Netherlands, Tech. Rep. APT536-10-0422, 2010.

[26] Q. Zou and S. Devasia, "Preview-based stable-inversion for output tracking of linear systems," *J. Dyn. Syst. Meas. Control*, vol. 121, no. 4, pp. 625–630, 1999.

[27] K. S. Ramani and C. E. Okwudire, "Regularized filtered basis functions approach for accurate tracking of discrete-time linear time invariant systems with bounded random uncertainties," in *Proc. ASME Dyn. Syst. Control Conf.*, 2016, Paper V002T28A004.
[28] K. S. Ramani and C. E. Okwudire, "Robust filtered basis functions approach for feedforward tracking control," in *Proc. ASME Dyn. Syst. Control Conf.*, 2018, Paper V003T35A003.
[29] J. A. Butterworth, L. Y. Pao, and D. Y. Abramovitch, "The effect of nonminimum-phase zero locations on the performance of feedforward model-inverse control techniques in discrete-time systems," in *Proc. Amer. Control Conf.*, 2008, pp. 2696–2702.
[30] L. Piegl, "On NURBS: A survey," *IEEE Comput. Graph. Appl.*, vol. 11, no. 1, pp. 55–71, Jan. 1991.
[31] K. S. Ramani, M. Duan, C. E. Okwudire, and A. G. Ulsoy, "Optimal selection of basis functions for minimum-effort tracking control of non-minimum phase systems using filtered basis functions," *J. Dyn. Syst. Meas. Control*, vol. 141, no. 11, 2019, Art. no. 111009.
[32] J. A. Butterworth, L. Y. Pao, and D. Y. Abramovitch, "Analysis and comparison of three discrete-time feedforward model-inverse control techniques for nonminimum-phase systems," *Mechatronics*, vol. 22, no. 5, pp. 577–587, Aug. 2012.
[33] S. Devasia, "Approximated stable inversion for nonlinear systems with nonhyperbolic internal dynamics," *IEEE Trans. Autom. Control*, vol. 44, no. 7, pp. 1419–1425, Jul. 1999.
[34] A. W. Bowman and A. Azzalini, *Applied Smoothing Techniques for Data Analysis: The Kernel Approach With S-Plus Illustrations*. London, U.K.: Oxford Univ. Press, 1997.
[35] C. Okwudire, S. Huggi, S. Supe, C. Huang, and B. Zeng, "Low-level control of 3D printers from the cloud: A step toward 3D printer control as a service," *Inventions*, vol. 3, no. 3, p. 56, 2018. http://dx.doi.org/10.3390/inventions3030056
[36] B. G. Dijkstra, "Iterative learning control with applications to a wafer stage," Doctoral dissertation, Mechanical Engineering, Delft Univ. Technol., Delft, The Netherlands, 2004.
[37] K. Hamamoto and T. Sugie, "An iterative learning control algorithm within prescribed input–output subspace," *Automatica*, vol. 37, no. 11, pp. 1803–1809, 2001.
[38] S. Gopinath, I. Kar, and R. Bhatt, "Wavelet series based learning controller design for kinematic path-tracking control of mobile robot," in *Proc. Int. Conf. Adv. Comput., Commun. Control*, 2009, vol. 35, pp. 129–135.
[39] L. Piegl and W. Tiller, *The NURBS Book*. New York, NY, USA: Springer, 1997.

Keval S. Ramani (Member, IEEE) received the B.E. degree in mechanical engineering from the Birla Institute of Technology and Science Pilani, Goa, India, in 2012, and the M.S. and Ph.D. degrees in mechanical engineering from the University of Michigan, Ann Arbor, MI, USA, in 2015 and 2019, respectively.

He is currently a Research Fellow with the Department of Mechanical Engineering, University of Michigan. From 2012 to 2013, he was with the Ingersoll Rand, Inc., Bengaluru, India, as an Engineering Trainee. He is the Co-Author of the Best Student Paper Award-winning paper on the FBF approach at the 2015 Dynamic Systems and Control Conference. His research interests include control, dynamics, vibration, and optimization, with application to manufacturing automation.

Nosakhare Edoimioya received the B.S. degree in mechanical engineering from Stanford University, Stanford, CA, USA, in 2017, and the M.S. degree in mechanical engineering in 2019 from the University of Michigan, Ann Arbor, MI, USA, where he is currently working toward the Ph.D. degree in mechanical engineering.

His current research focuses on mechatronics systems design for improved performance of additive manufacturing machines.

Mr. Edoimioya was the recipient of the National Science Foundation GRFP Award in 2018.

Chinedum E. Okwudire (Member, IEEE) received the Ph.D. degree in mechanical engineering from The University of British Columbia, Vancouver, BC, Canada, in 2009.

In 2011, he joined the Mechanical Engineering Faculty with the University of Michigan, Ann Arbor, MI, USA. Prior to joining the University of Michigan, he was the Mechatronic Systems Optimization Team Leader with DMG Mori USA Inc., Davis, CA, USA. His research interests include smart and sustainable automation, where he leverages the fundamental engineering disciplines of machine design, structural dynamics, and control theory to tackle challenging problems in precision, throughput, and energy efficiency faced in manufacturing automation.

Dr. Okwudire was the Recipient of the International Symposium on Flexible Automation Young Investigator Award, the Society of Manufacturing Engineers Outstanding Young Manufacturing Engineer Award, the SAE International Ralph Teetor Educational Award; the National Science Foundation CAREER Award, and the 2016 ASME Dynamic Systems and Controls Division's Best Conference Paper in Mechatronics Award.